

Growth and Characterization of PDMS-Stamped Halide Perovskite Single Microcrystals

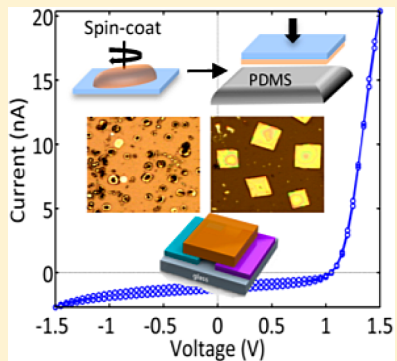
Parisa Khoram,[†] Sarah Brittman,[†] Wojciech I. Dzik,[‡] Joost N. H. Reek,[‡] and Erik C. Garnett*,[†]

[†]Center for Nanophotonics, FOM Institute AMOLF, Science Park 104, 1098 XG Amsterdam, The Netherlands

[‡]Homogeneous, Supramolecular & Bio-Inspired Catalysis van't Hoff Institute for Molecular Sciences, University of Amsterdam, P.O. Box 94720, 1090 GE Amsterdam, The Netherlands

Supporting Information

ABSTRACT: Recently, halide perovskites have attracted considerable attention for optoelectronic applications, but further progress in this field requires a thorough understanding of the fundamental properties of these materials. Studying perovskites in their single-crystalline form provides a model system for building such an understanding. In this work, a simple solution-processed method combined with PDMS (polydimethylsiloxane) stamping was used to prepare thin single microcrystals of halide perovskites. The method is general for a broad array of materials including $\text{CH}_3\text{NH}_3\text{PbBr}_3$, $\text{CH}_3\text{NH}_3\text{PbCl}_3$, $\text{CH}_3\text{NH}_3\text{Pb}(\text{Br}_{0.5}\text{Cl}_{0.5})_3$, $\text{CH}_3\text{NH}_3\text{Pb}(\text{Br}_{0.75}\text{Cl}_{0.25})_3$, CsPbBr_3 , $\text{Cs}_3\text{Bi}_2\text{Br}_9$, and $\text{Cs}_3\text{Bi}_2\text{I}_9$. Electron backscatter diffraction (EBSD) was used to investigate the microstructure of the crystals. In order to characterize the microcrystals of $\text{CH}_3\text{NH}_3\text{PbBr}_3$ electrically, the crystals were grown on prefabricated electrodes creating single-crystal devices contacted from the back. This back-contacted platform circumvents the incompatibility between halide perovskites and the aqueous chemistry used in standard microfabrication processes. It also allows *in situ* characterization of the perovskite crystal while it operates as a microscopic solar cell.



INTRODUCTION

Since the introduction of organolead trihalide perovskites as the light-absorbing semiconductor in solar cells,¹ much effort has been devoted to the development of these materials for optoelectronic applications.^{2–5} This is due to their high efficiency and inexpensive, solution-based processing. So far, the efforts in this field have led to power conversion efficiencies exceeding 20% for solar cells based on $\text{CH}_3\text{NH}_3\text{PbI}_3$.⁶

The perovskites with formula AMX_3 are crystalline materials in which A and M are cations of different sizes and X is an anion. To date, most of the work on organic–inorganic hybrid perovskites has focused on materials with A = methylammonium (CH_3NH_3^+), M = lead (Pb^{2+}), and X = Cl^- , Br^- , I^- , or a mixture of these halides. Mixtures of neighboring anions (e.g., $\text{I}-\text{Br}$ and $\text{Br}-\text{Cl}$) can be produced to tune the band gap from that of pure $\text{CH}_3\text{NH}_3\text{PbI}_3$ (~1.5 eV) to $\text{CH}_3\text{NH}_3\text{PbCl}_3$ (~3.1 eV).^{6–8} $\text{CH}_3\text{NH}_3\text{PbBr}_3$ (~2.2 eV) sits in the middle of this range, making it and mixtures of it with $\text{CH}_3\text{NH}_3\text{PbCl}_3$ suitable for light-emission applications such as lasing⁹ and light-emitting diodes (LEDs).^{10,11} Mixtures of $\text{CH}_3\text{NH}_3\text{PbBr}_3$ with $\text{CH}_3\text{NH}_3\text{PbI}_3$ are appropriate for solar cells with high open-circuit voltage (V_{oc})^{12–15} and the upper cell in multijunction photovoltaics. Apart from hybrid organic–inorganic perovskites, all-inorganic halide perovskites such as CsPbBr_3 (with a band gap of ~2.4 eV) have also shown promise for photovoltaics and light-emitting diodes.^{16,17}

Because the microstructure and crystallinity of hybrid perovskites are known to affect their properties¹⁸ and

performance in solar cells,¹⁹ it is important to study single crystalline perovskites free of grain boundaries.²⁰ Only a few previous studies have examined single crystalline hybrid perovskites.^{21–29} In these works the perovskite crystals were formed by slow crystallization processes, such as antisolvent vapor-assisted crystallization,²¹ top-seeded-solution-growth,²² or solvothermal growth.²³ These processes are unlike the rapid crystallization that occurs during the drying of the spin-coated films commonly used in solar cells. Also, the crystals' thicknesses of several millimeters were far from those relevant for optoelectronic devices. Therefore, these previous studies focused primarily on the photophysical and optical properties of single crystals,^{25,27} although Shi et al. and Dong et al. did fabricate electrodes on the top and bottom of their thick single crystals to investigate charge carrier dynamics.^{21,22}

Here we fabricated single-crystalline halide perovskites by applying the typical method of spin-coating from solution used to make polycrystalline thin films. A PDMS-stamping step confined the solution during evaporation of the solvent and resulted in the formation of individual crystals. The typical thickness of the crystals grown by this method (~500 nm to a few micrometers, depending on the processing conditions) is much closer to what is commonly used in high-performance optoelectronic devices and can be reduced further to ~100 nm

Received: February 26, 2016

Revised: March 7, 2016

Published: March 9, 2016

by adjusting the deposition conditions.³⁰ This method is general and can be applied to form thin single crystals of a variety of hybrid, inorganic, and lead-free halide perovskites.

■ EXPERIMENTAL METHODS

Preparation of Methylammonium Halide ($\text{CH}_3\text{NH}_3\text{X}$, X = Br or Cl). $\text{CH}_3\text{NH}_3\text{X}$ was synthesized by the addition of hydrobromic acid (48 wt % in H_2O , Sigma-Aldrich) or hydrochloric acid (37 wt % in H_2O , Sigma-Aldrich) dropwise into methylamine (33 wt % in EtOH, Sigma-Aldrich) while it was stirring in an ice bath. After stirring for 2 h in the ice bath, the solution was removed and heated to 150 °C to evaporate off the solvents, while stirring was continued. The resulting powder, either white or occasionally pale yellow, was recrystallized from ethanol. The final white crystals of $\text{CH}_3\text{NH}_3\text{X}$ were dried by heating at 100–150 °C in air.

Preparation of Halide Perovskite Solutions. All solutions were prepared at room temperature and in air. To prepare pure $\text{CH}_3\text{NH}_3\text{PbBr}_3$ crystals, PbBr_2 (Sigma-Aldrich, purity ≥98%) was mixed in a 1:1 molar ratio with $\text{CH}_3\text{NH}_3\text{Br}$ in dimethylformamide (DMF) (Sigma-Aldrich, anhydrous, 99.8%) or dimethyl sulfoxide (DMSO) (Sigma-Aldrich, anhydrous, purity ≥ 99.5%). For pure $\text{CH}_3\text{NH}_3\text{PbCl}_3$ crystals, PbCl_2 (Sigma-Aldrich, purity ≥98%) and $\text{CH}_3\text{NH}_3\text{Cl}$ were mixed in a 1:1 molar ratio in DMSO at 1 M concentration. To prepare mixed halide ($\text{CH}_3\text{NH}_3\text{Pb}(\text{Br}_{0.5}\text{Cl}_{0.5})_3$ and $\text{CH}_3\text{NH}_3\text{Pb}(\text{Br}_{0.75}\text{Cl}_{0.25})_3$) solutions, pure 1 M solutions of $\text{CH}_3\text{NH}_3\text{PbBr}_3$ and $\text{CH}_3\text{NH}_3\text{PbCl}_3$ in DMSO were mixed in the desired stoichiometric ratio (1:1 or 3:1). For making the all-inorganic CsPbBr_3 solution, CsBr (Sigma-Aldrich, 99.999%) and PbBr_2 precursors were mixed in a stoichiometric ratio in DMSO (0.33 M solution). $\text{Cs}_3\text{Bi}_2\text{I}_9$ and $\text{Cs}_3\text{Bi}_2\text{Br}_9$ solutions were made by mixing CsBr with BiBr_3 (Sigma-Aldrich, purity ≥98%) and CsI (Sigma-Aldrich, 99.9%) with BiI_3 (Sigma-Aldrich, 99%) in a stoichiometric ratio in DMSO (concentrations well below 1 M). The fresh solutions were ultrasonicated for 5 min to ensure full dissolution of the precursors prior to deposition.

Fabrication of Single Crystals. The perovskite solution was spin coated on fused silica substrates. The substrates were cleaned with acetone, isopropanol, and O_2 plasma prior to the deposition. A RIE/ICP plasma etcher from Oxford Instruments (Plasmalab 80 plus) was used to remove contamination and treat the surface of the substrates. The process parameters were as follows: O_2 flow of 25 sccm, pressure of 30 mTorr, and forward power of 50 W for 2 min. The spinning speed and time were adjusted to prevent the full evaporation of the solvent (10 s at 500 rpm for DMF solutions and 30–60 s at 2000–4000 rpm for DMSO solutions). The wet substrate was immediately pressed face down onto a piece of PDMS on a hot plate held at 100 °C (for DMF solutions) or 150 °C (for DMSO solutions) for 2–5 min, until the crystals formed and the substrate changed color. Inorganic perovskites in DMSO were annealed at 150–200 °C. After the crystals were formed on the substrate in contact with PDMS, the sample was removed from the PDMS and annealed for about 10 min face up to ensure the evaporation of excess solvent. The PDMS stamp was fabricated by mixing the monomer and curing agent (10:1 ratio, SYLGRAD 184, Dow Corning) and curing on a piece of clean Si wafer. The side formed in contact with the Si was always used to stamp the crystals. PDMS stamps were reused after cleaning the surface by ultrasonication in water and a rinse in isopropanol.

Back-Contacted Electrode Fabrication. The electrodes were fabricated on glass substrates by a two-step photolithography process. Glass substrates were cleaned in acetone and isopropanol prior to spin coating with photoresist. In the first step, one set of electrodes was patterned, and the metal was deposited by electron-beam or thermal evaporation, followed by lift-off in acetone. The second lithography step was repeated as the first one, using alignment markers to adjust the gap between the electrodes. Another metal was then deposited. In the case of symmetric devices, the lithography was done in one step. The thickness of the metals was 100 nm.

Device Fabrication. To make $\text{CH}_3\text{NH}_3\text{PbBr}_3$ back-contacted devices, the same procedure of spin coating the precursor solution followed by PDMS stamping was applied using substrates with prefabricated electrodes. To fabricate the devices, O_2 plasma cleaning of substrates was necessary to form consistent contacts. Using a lower powered table-top plasma cleaner to prepare the electrodes resulted in inferior devices.

Atomic Force Microscopy (AFM). AFM images were taken by a Veeco Dimension 3100 in tapping mode.

Scanning Electron Microscopy (SEM). SEM images were taken by a FEI Verios 460 at 5 kV accelerating voltage, in secondary electron mode, and under a 30° tilt.

Electron Backscatter Diffraction (EBSD). The EBSD setup was built in a FEI XL30 S FEG. The patterns were collected using 20 kV accelerating voltage. The sample was tilted 70°. The patterns were indexed using Delphi 2 software from EDAX. The system was calibrated prior to indexing with Si (100).

Device Characterization. I – V curves were measured with an Agilent B2902A source-measure unit. To simulate solar illumination, an Oriel Sol2A Class ABA Solar Simulator from Newport was used. 1 sun intensity was calibrated using a silicon reference cell (Newport 91150 V).

Scanning Photocurrent Mapping. The photocurrent maps were taken using a home-built optical setup consisting of a supercontinuum Fianium WL-SC390-3 laser, sent through an acousto-optic tunable filter (Fianium AOTF-V1-N1). The wavelength could be selected based on the experiment from 410 to 750 nm. The beam was focused through the objective (Mitutoyo M PLAN APO NUV 50×, NA 0.42) onto the mounted substrate. The spot radius was ~650 nm. The sample was electrically wire-bonded to a printed circuit board specially designed for the setup and scanned spatially with the focused laser beam using a piezoelectric stage (Piezosystem Jena Tritor 400 CAP). The photocurrent was measured with the same source-measure unit as used for I – V measurements. The voltage on the sample was scanned from 0 up to 2 V and then returned to zero prior to measuring the photocurrent map, and the mapping was done while the sample was kept at the short-circuit condition. The reflected beam power was measured simultaneously with a Thorlabs amplified photodiode (PDA100A) to correlate the position with the current in the superimposed maps. A silicon photodetector (Newport model 818-UV-L) was used to measure the absolute beam power in each measurement.

■ RESULTS AND DISCUSSION

Flat and smooth halide perovskite crystals were produced by combining solution deposition with a PDMS-stamping technique. To form the crystals, a stoichiometric solution of the perovskite precursors ($\text{CH}_3\text{NH}_3\text{Br}$, $\text{CH}_3\text{NH}_3\text{Cl}$, CsBr , or CsI and PbBr_2 , PbCl_2 , BiBr_3 , or BiI_3) in dimethylformamide

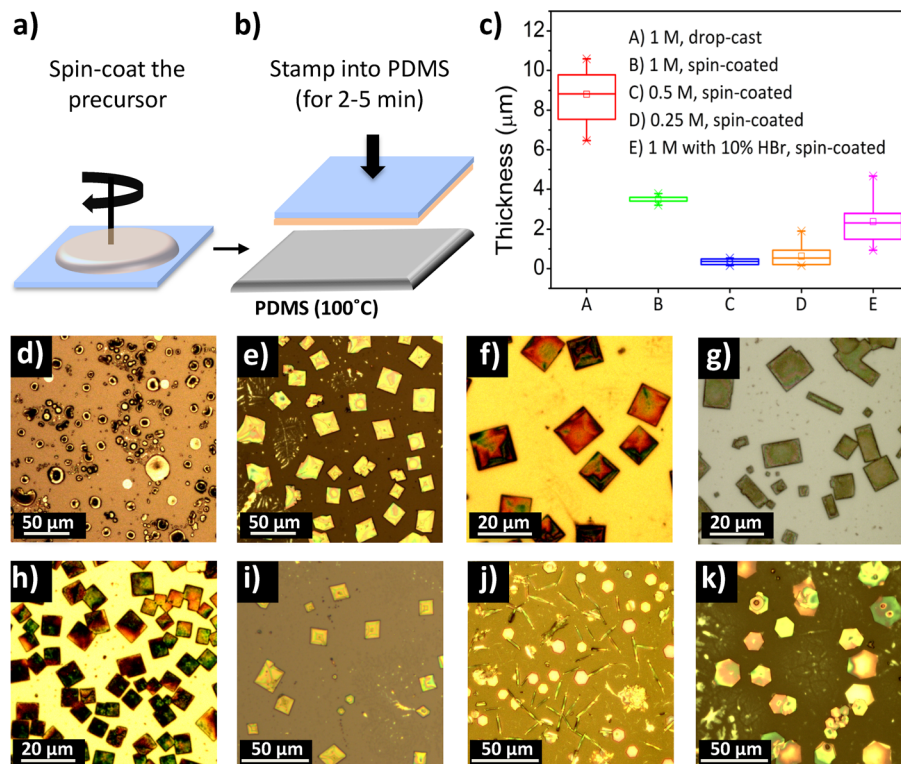


Figure 1. PDMS-stamping technique for fabrication of smooth and thin halide perovskites. (a) Spin-coating of solution on top of the prepared platform. The solvent was not allowed to evaporate fully. (b) Pressing the substrate face down into PDMS on a hot plate ($100\text{ }^{\circ}\text{C}$) until the crystals formed. (c) Controlling the thickness of $\text{CH}_3\text{NH}_3\text{PbBr}_3$ crystals. All samples were prepared by deposition of freshly prepared $\text{CH}_3\text{NH}_3\text{PbBr}_3$ precursor solution in DMF with varied concentrations onto a glass substrate via the listed technique (drop-cast or spin-coated). For sample E, 10 vol % of hydrobromic acid (HBr) (48% in H_2O) was added to the solution. (d) Optical microscopy image of $\text{CH}_3\text{NH}_3\text{PbBr}_3$ crystals deposited by spin-coating of solution on a glass substrate without PDMS-stamping. (e) Optical microscopy image of $\text{CH}_3\text{NH}_3\text{PbBr}_3$, (f) $\text{CH}_3\text{NH}_3\text{PbCl}_3$, (g) $\text{CH}_3\text{NH}_3\text{Pb}(\text{Br}_{0.75}\text{Cl}_{0.25})_3$, (h) $\text{CH}_3\text{NH}_3\text{Pb}(\text{Br}_{0.5}\text{Cl}_{0.5})_3$, (i) CsPbBr_3 , (j) $\text{Cs}_3\text{Bi}_2\text{Br}_9$, and (k) $\text{Cs}_3\text{Bi}_2\text{I}_9$ crystals fabricated by spin-coating of solution on glass, followed by PDMS-stamping.

(DMF) or dimethyl sulfoxide (DMSO) was spin-coated onto the substrate. Prior to deposition of the solution, the substrate was cleaned with an O_2 plasma, which made it hydrophilic. Immediately after the deposition of the solution, the substrate was pressed face down into a piece of PDMS heated on a hot plate ($100\text{--}200\text{ }^{\circ}\text{C}$) until the solvent had evaporated (Figure 1a,b). Individual crystals formed randomly on the substrate, and crystallizing in contact with the flat surface of the PDMS created faceted, smooth crystals with thicknesses of a few micrometers to hundreds of nanometers, depending on the deposition conditions (Figure 1c). If the PDMS-stamping step was not applied, rapid evaporation of the solvent in the absence of PDMS produced unshaped crystals with very rough surfaces (Figure 1d,e). Atomic force microscopy (AFM) of the surface of several $\text{CH}_3\text{NH}_3\text{PbBr}_3$ crystals indicated that the root-mean-square (rms) roughness was $7.1 \pm 4.6\text{ nm}$ as compared to $79.1 \pm 43.3\text{ nm}$ for crystals formed without stamping (Figure S1).

The morphology of the crystals, including their size and thickness, was influenced by several parameters, such as the concentration of the precursor solution, additives to the solution such as hydrobromic acid, and the method of deposition of the solution before stamping (e.g., drop-casting or spin-coating). The crystals, however, were not produced uniformly over the entire substrate, likely because pressure was applied nonuniformly across the substrate; therefore, in each sample at least five crystals were measured on the substrate using either a profilometer or an atomic force microscope (AFM). Because of this sampling procedure, the chart boxes

that compare the thicknesses of the crystals fabricated by different parameters are not necessarily representative of the thickness variations over each substrate. In general, however, a lower concentration of solution gave a majority of thinner crystals (below $1\text{ }\mu\text{m}$), but the lateral dimensions of the crystals decreased as well. Addition of HBr or using DMSO as the solvent³⁰ decreased the thickness of $\text{CH}_3\text{NH}_3\text{PbBr}_3$ crystals. Spin-coating also provided a more uniform size distribution than drop-casting.

This method is broadly applicable to produce smooth single crystals of a library of halide perovskites. In addition to crystals of $\text{CH}_3\text{NH}_3\text{PbBr}_3$, PDMS-stamped microcrystals of $\text{CH}_3\text{NH}_3\text{PbCl}_3$ and mixed halides ($\text{CH}_3\text{NH}_3\text{Pb}(\text{Br}_{0.5}\text{Cl}_{0.5})_3$ and $\text{CH}_3\text{NH}_3\text{Pb}(\text{Br}_{0.75}\text{Cl}_{0.25})_3$) were also generated (Figure 1f-h). By varying the spin conditions and annealing temperatures, this method also produced crystals of a variety of other perovskites, including inorganic CsPbBr_3 and lead-free, hexagonal perovskites such as $\text{Cs}_3\text{Bi}_2\text{I}_9$ and $\text{Cs}_3\text{Bi}_2\text{Br}_9$ (Figure 1i-j).

The individual crystals of $\text{CH}_3\text{NH}_3\text{PbBr}_3$ formed by PDMS-stamping are typically single crystals with a faceted, square-prismatic shape. The smoothness of their surface allows the identification of the orientation and domains of the crystals by electron backscatter diffraction (EBSD) (Figure 2). EBSD is a SEM-based technique that is well established to determine the crystallographic orientations of microstructures.^{31,32} In this technique, the focused electron beam strikes the surface of the crystal at a high angle (here, 70°). Electrons scattered from the

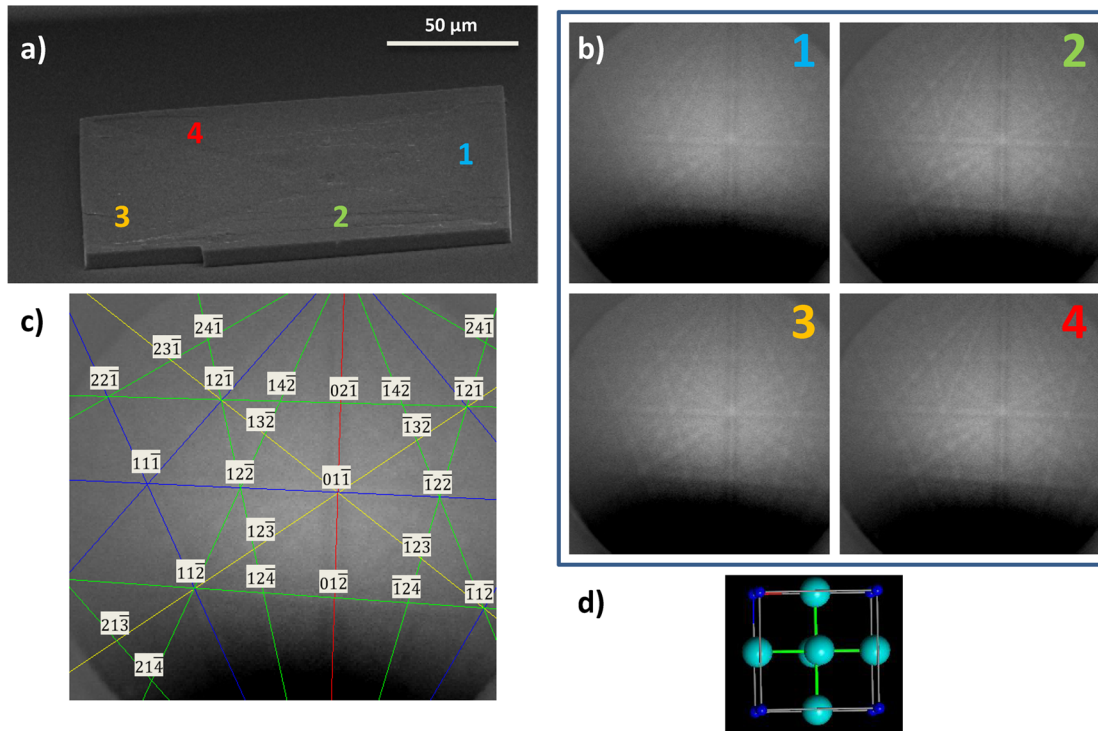


Figure 2. Electron backscatter diffraction (EBSD) of a $\text{CH}_3\text{NH}_3\text{PbBr}_3$ single crystal. (a) SEM image of a $\text{CH}_3\text{NH}_3\text{PbBr}_3$ single crystal. Numbers indicate the positions of the electron beam where the EBSD patterns were collected. (b) EBSD patterns from four different locations on the crystal, which all show the same Kikuchi pattern indicating the same crystallographic orientation. Each pattern is related to the location with the similar number in (a). (c) Indexed EBSD pattern. (d) The orientation of the surface of the $\text{CH}_3\text{NH}_3\text{PbBr}_3$ crystal is $\langle 100 \rangle$, extracted from the indexed EBSD pattern. Green spheres are bromide anions, while blue spheres are the methylammonium cations.

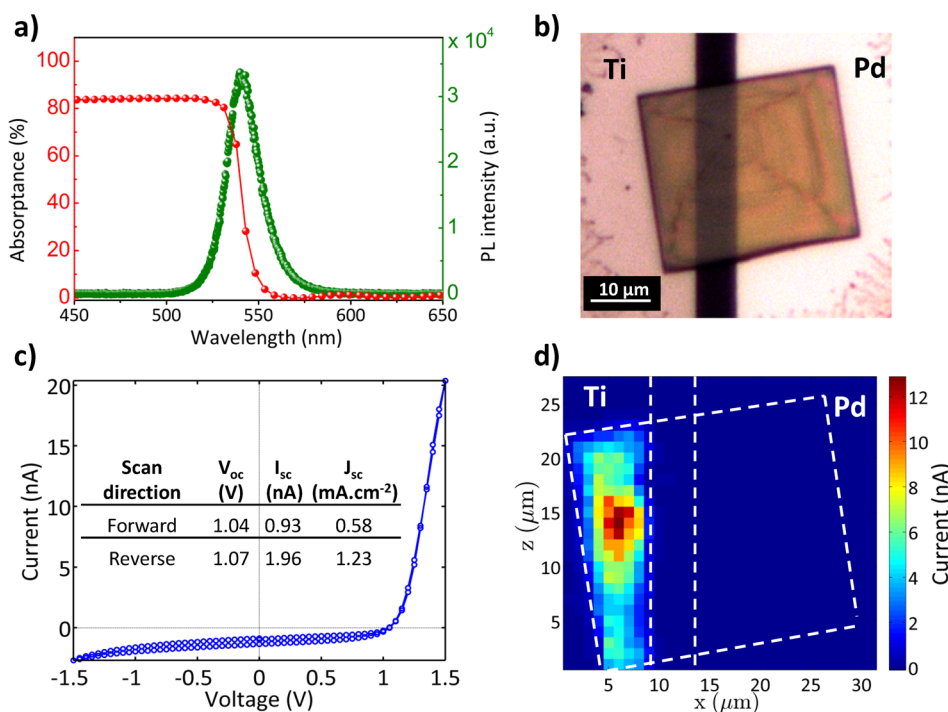


Figure 3. Optical and electrical characterization of a $\text{CH}_3\text{NH}_3\text{PbBr}_3$ single crystal. (a) Absorption (red) and photoluminescence (PL) (green) spectra of a $\text{CH}_3\text{NH}_3\text{PbBr}_3$ single crystal prepared by the PDMS-stamping technique. (b) Optical microscopy image of a $\text{CH}_3\text{NH}_3\text{PbBr}_3$ single crystal prepared on a prefabricated back-contacted electrode platform. (c) $I-V$ characteristic of the $\text{CH}_3\text{NH}_3\text{PbBr}_3$ single crystal device in (b) under 1 sun illumination. Inset shows the photovoltaic performance of the device in the forward and reverse scan directions (scan rate 0.1 V/s). (d) Scanning photocurrent map of the same crystal in (b) ($\lambda = 540 \text{ nm}$, $\sim 250 \text{ W cm}^{-2}$). Dashed lines indicate the position of the electrodes, drawn from the superimposed photocurrent map and optical image (Figure S10).

surface form a diffraction pattern, called a Kikuchi pattern because of its prominent Kikuchi bands.³² Several positions on the surface of each smooth crystal of $\text{CH}_3\text{NH}_3\text{PbBr}_3$ were measured (Figure 2a). The Kikuchi patterns from these positions (Figure 2b) were similar, indicating that there are no grain boundaries within the crystal. Indexing the Kikuchi patterns (Figure 2c) for 14 different single crystals showed that the surface plane is (100) (Figure 2d). Single-crystal X-ray diffraction confirmed the single crystallinity of the square crystals (Supporting Information). Although many of the crystals formed using PDMS-stamping were square prisms, others displayed a line along their diagonal (Figure S2). EBSD patterns taken from opposite sides of the line were dissimilar, indicating that the line is a grain boundary between a $\langle 100 \rangle$ domain and a $\langle 110 \rangle$ domain. EBSD was also used to analyze the microstructure of CsPbBr_3 PDMS-stamped crystals, which were also typically single crystals (Supporting Information).

Optical characterization of the PDMS-stamped single crystals of $\text{CH}_3\text{NH}_3\text{PbBr}_3$ was performed by diffraction-limited absorption and photoluminescence (PL) measurements (excitation wavelength of 405 nm) (Figure 3a) on a $1 \mu\text{m}$ thick crystal. The PL spectrum, which was collected in reflection, shows a narrow emission peak centered around 540 nm (2.29 eV). The onset of absorption is red-shifted and located at ~ 555 nm (2.25 eV). Controlling the thickness of the crystals allowed the measurement of the material's complex refractive index from 405 to 1100 nm, which agreed well with values measured on macroscopic single crystals.³⁰

To characterize the $\text{CH}_3\text{NH}_3\text{PbBr}_3$ single crystals electrically, the crystals must be contacted by metal electrodes; however, standard lithographic techniques require processing substrates in aqueous solutions, which will dissolve the ionic perovskite crystals. For this reason, electrodes were fabricated on the substrate using photolithography prior to the growth of the crystals (Supporting Information). The first requirement for the electrodes is their appropriate energy band alignment relative to the bands of the perovskite. The valence and conduction band edges of $\text{CH}_3\text{NH}_3\text{PbBr}_3$ have been reported as 5.9 and 3.6 eV, respectively.³³ Based on these band positions, several metals were candidates for electron- or hole-selective electrodes.³⁴ In the back-contacted geometry, however, the perovskite crystals are deposited on top of the electrodes, so the metals of the electrodes should be chemically inert in the solution containing the perovskite's precursors and in contact with the perovskite itself. TiO_2 is the common electron transporter material used in conventional planar perovskite solar cells,³⁵ therefore, titanium was a clear choice for the electron-selective contact. A thin titanium oxide layer forms on the surface of Ti metal and likely prevents any chemical reactions between the perovskite and the underlying metal. Palladium was chosen as the hole-selective contact (Figure S6), and no damage to the electrodes were observed after deposition of the crystals or during measurements. Further details regarding the selection of electrode materials are given in the Supporting Information.

To produce solar cells, back-contacted devices with asymmetric contacts (Ti–Pd) were fabricated, followed by deposition of the perovskite crystals (Figure 3b). Current–voltage (I – V) curves of the devices were measured in the dark (Figure S9) and under illumination with a standard light source (AM 1.5G, 100 mW cm^{-2} irradiance) (Figure 3c). The devices displayed rectifying I – V curves both in the dark and under illumination. A champion back-contacted single crystal solar

cell had an open-circuit voltage (V_{oc}) of 1.04 and 1.07 V in forward and reverse scans, respectively, better than the V_{oc} of the first demonstration of planar $\text{CH}_3\text{NH}_3\text{PbBr}_3$ perovskite solar cells in the literature¹⁴ (0.84 V) but somewhat lower than cells with more optimized hole-selective layers (1.3 V)¹⁴ and later studies (1.4 and 1.51 V).^{12,13} The single crystal $\text{CH}_3\text{NH}_3\text{PbBr}_3$ solar cell exhibited a short circuit current (I_{sc}) of 0.93 and 1.96 nA in forward and reverse scan directions, respectively, which is equivalent to 0.58 and 1.23 mA cm^{-2} short circuit current density (J_{sc}). The J_{sc} was calculated by considering the overlapped area of the crystal with the Ti electrode as the active area, according to photocurrent mapping (Figure 3c). Again, these values are comparable to those of early planar $\text{CH}_3\text{NH}_3\text{PbBr}_3$ perovskite solar cells (1.08 mA cm^{-2})¹⁴ although later studies^{12,13} with improved hole transporter layers¹³ and improving surface coverage of the $\text{CH}_3\text{NH}_3\text{PbBr}_3$ ¹² demonstrated much higher J_{sc} values (6.1¹³ and 8.4¹² mA cm^{-2}). These reports show the importance of the hole transporter layer and suggest that the back-contacted single crystal $\text{CH}_3\text{NH}_3\text{PbBr}_3$ solar cell performance will improve substantially with deposition of proper charge transporter layers.

To investigate the spatial distribution of the photocurrent within the device, scanning photocurrent mapping using laser illumination (power density $\sim 250 \text{ W cm}^{-2}$ at 540 nm) was applied (Figure 3c). The positions of the crystal and electrodes were correlated to the photocurrent map by superimposing the reflectance map of the crystal taken simultaneously with the photocurrent map and the optical image (Figure S10). This correlation shows that the photocurrent originates only from the region of the crystal directly above the Ti electrode. Moreover, not all of the area above this electrode is equally active.

The observation of current localized to the electron-selective Ti contact suggests a short diffusion length for electrons in $\text{CH}_3\text{NH}_3\text{PbBr}_3$. In the case of illumination near the hole-selective electrode, electrons must travel laterally through the width of the gap between the electrodes (few microns) to be collected by the Ti contact. If their diffusion length is shorter than this width, they recombine before being collected; therefore, regions of the crystal far from the titanium electrode appear inactive. When the crystal is illuminated near the electron-selective contact, electrons must travel only the vertical distance between their position of excitation and the electrode. Since this crystal is relatively thin ($\sim 1 \mu\text{m}$) and the energy of the incident photons (2.29 eV) is close to the band gap of $\text{CH}_3\text{NH}_3\text{PbBr}_3$ (~ 2.2 eV), some electron–hole pairs are generated close enough to the back contact for the electrons to be collected. The lack of significant lateral current decay from the edge of the electrode indicates that the carrier diffusion length is smaller than the size of the optical spot, approximately 1 μm . This short electron diffusion length is consistent with predictions of p-type conductivity in $\text{CH}_3\text{NH}_3\text{PbBr}_3$ ³⁶ and reported electron diffusion lengths in polycrystalline films of ~ 100 nm (in dark) and ~ 360 nm (under 0.03–0.04 sun illumination), which were measured by electron-beam-induced current (EBIC).³⁷ In millimeter-sized single crystals, Shi et al. reported much longer diffusion lengths (~ 3 – $17 \mu\text{m}$) determined by measuring the mobility and photoluminescence lifetime of their crystals.²¹ These larger crystals grown by slow precipitation over several days likely have fewer defects than the perovskite deposited by rapid

precipitation after spin-coating, yielding a longer diffusion length.

The second observation in the photocurrent map of the $\text{CH}_3\text{NH}_3\text{PbBr}_3$ single crystal is the nonuniformity of the photocurrent over the Ti contact. The locations of hot spots on the photocurrent map vary for different measured crystals (Figure S11). While most of the region on the Ti electrode produces more than 3 nA of current, some regions produce as much as 4 times that amount. Because the photocurrent map is a convolution of light absorption and charge collection, the variations could arise from either process. For thin crystals, changes in thickness can lead to dramatic variations in photocurrent because absorption is enhanced or suppressed by thin-film interference; however, a simple one-dimensional model (Figure S12) based on the AFM-measured thicknesses in this crystal (Figure S13) indicates that the observed variations are too large to arise from interference effects alone. Variations in the efficiency of charge collection could also contribute to this inhomogeneity and might result from a nonuniform interface between the electrode and perovskite. For example, the nucleation site of the crystal might produce the most intimate contact with the electrode, which could locally enhance the efficiency of charge collection. Differences in the thickness or chemical composition of the titanium oxide layer on the surface of the electrode could also influence the local collection efficiency and yield the observed variations in photocurrent.

CONCLUSIONS

In summary, we have introduced a simple technique to create smooth, thin halide perovskite microcrystals by combining single-step deposition of precursors from solution with PDMS-stamping. This method is general for making a variety of halide perovskites, including hybrid, all-inorganic, and lead-free hexagonal perovskites. Because of the smooth surface of the crystals, EBSD could be used to identify the microstructure of $\text{CH}_3\text{NH}_3\text{PbBr}_3$ crystals, which typically exhibited a (100) surface facet. These single crystals are ideal for studying perovskite optoelectronic devices on a fundamental level. To this end, the crystals were electrically contacted from the back to avoid any postgrowth fabrication steps that might damage the crystals. We used this back-contacted platform to investigate the photovoltaic performance of single-crystal $\text{CH}_3\text{NH}_3\text{PbBr}_3$ and performed photocurrent mapping of the device to understand the spatial distribution of its photo-generated current. The photocurrent originated from the portion of the crystal directly above the electron-selective contact, suggesting these $\text{CH}_3\text{NH}_3\text{PbBr}_3$ single crystals are p-type and have an electron diffusion length below 1 μm . This PDMS-stamping approach, together with the back-contacted platform for electrical characterization, provides a unique tool to investigate the optoelectronic properties of a variety of single-crystalline halide perovskites.

ASSOCIATED CONTENT

Supporting Information

The Supporting Information is available free of charge on the ACS Publications website at DOI: [10.1021/acs.jpcc.6b02011](https://doi.org/10.1021/acs.jpcc.6b02011).

Morphology and EBSD of stamped $\text{CH}_3\text{NH}_3\text{PbBr}_3$ and CsPbBr_3 crystals, single-crystal X-ray diffraction of $\text{CH}_3\text{NH}_3\text{PbBr}_3$, fabrication of back-contacted solar cells and investigations of other metal electrodes, super-

imposed optical image and photocurrent map, photocurrent maps of several other single-crystal $\text{CH}_3\text{NH}_3\text{PbBr}_3$ solar cells, and model of the photocurrent in the $\text{CH}_3\text{NH}_3\text{PbBr}_3$ crystal ([PDF](#))

AUTHOR INFORMATION

Corresponding Author

*(E.C.G.) Tel +31–20 754 7231; e-mail garnett@amolf.nl.

Notes

The authors declare no competing financial interest.

ACKNOWLEDGMENTS

The authors thank Dr. Mark Knight and Dr. Artem Bakulin for helpful comments on the manuscript and Andries Lof for assistance in EBSD measurements. This work is part of the research program of the Foundation for Fundamental Research on Matter (FOM), which is part of The Netherlands Organization for Scientific Research (NWO). The authors acknowledge financial support from the European Research Council under the European Union's Seventh Framework Programme (FP/2007–2013)/ERC Grant Agreement No. 337328, "NanoEnabledPV", and from an industrial partnership between Philips and FOM.

REFERENCES

- (1) Kojima, A.; Teshima, K.; Shirai, Y.; Miyasaka, T. Organometal Halide Perovskites as Visible-Light Sensitizers for Photovoltaic Cells. *J. Am. Chem. Soc.* **2009**, *131*, 6050–6051.
- (2) Green, M. A.; Ho-Baillie, A.; Snaith, H. J. The Emergence of Perovskite Solar Cells. *Nat. Photonics* **2014**, *8*, 506–514.
- (3) Snaith, H. J. Perovskites: The Emergence of a New Era for Low-Cost, High-Efficiency Solar Cells. *J. Phys. Chem. Lett.* **2013**, *4*, 3623–3630.
- (4) Stranks, S. D.; Snaith, H. J. Metal-Halide Perovskites for Photovoltaic and Light-Emitting Devices. *Nat. Nanotechnol.* **2015**, *10*, 391–402.
- (5) Brittman, S.; Adhyaksa, G. W. P.; Garnett, E. C. The Expanding World of Hybrid Perovskites: Materials Properties and Emerging Applications. *MRS Commun.* **2015**, *5*, 7–26.
- (6) Jeon, N. J.; Noh, J. H.; Yang, W. S.; Kim, Y. C.; Ryu, S.; Seo, J.; Seok, S. I. Compositional Engineering of Perovskite Materials for High-Performance Solar Cells. *Nature* **2015**, *517*, 476–480.
- (7) Noh, J. H.; Im, S. H.; Heo, J. H.; Mandal, T. N.; Seok, S. I. Chemical Management for Colorful, Efficient, and Stable Inorganic–Organic Hybrid Nanostructured Solar Cells. *Nano Lett.* **2013**, *13*, 1764–1769.
- (8) Amat, A.; Mosconi, E.; Ronca, E.; Quarti, C.; Umari, P.; Nazeeruddin, M. K.; Grätzel, M.; De Angelis, F. Cation-Induced Band-Gap Tuning in Organohalide Perovskites: Interplay of Spin–Orbit Coupling and Octahedra Tilting. *Nano Lett.* **2014**, *14*, 3608–3616.
- (9) Xing, G.; Mathews, N.; Lim, S. S.; Yantara, N.; Liu, X.; Sabba, D.; Grätzel, M.; Mhaisalkar, S.; Sum, T. C. Low-Temperature Solution-Processed Wavelength-Tunable Perovskites for Lasing. *Nat. Mater.* **2014**, *13*, 476–480.
- (10) Tan, Z.-K.; et al. Bright Light-Emitting Diodes Based on Organometal Halide Perovskite. *Nat. Nanotechnol.* **2014**, *9*, 687–692.
- (11) Kim, Y. H.; Cho, H.; Heo, J. H.; Kim, T. S.; Myoung, N.; Lee, C. L.; Im, S. H.; Lee, T. W. Multicolored Organic/Inorganic Hybrid Perovskite Light-Emitting Diodes. *Adv. Mater.* **2015**, *27*, 1248–1254.
- (12) Heo, J. H.; Song, D. H.; Im, S. H. Planar $\text{CH}_3\text{NH}_3\text{PbBr}_3$ Hybrid Solar Cells with 10.4% Power Conversion Efficiency, Fabricated by Controlled Crystallization in the Spin-Coating Process. *Adv. Mater.* **2014**, *26*, 8179–8183.
- (13) Ryu, S.; Noh, J. H.; Jeon, N. J.; Kim, Y. C.; Yang, S.; Seo, J. W.; Seok, S. I. Voltage Output of Efficient Perovskite Solar Cells with High

- Open-Circuit Voltage and Fill Factor. *Energy Environ. Sci.* **2014**, *7*, 2614–2618.
- (14) Edri, E.; Kirmayer, S.; Cahen, D.; Hodes, G. High Open-Circuit Voltage Solar Cells Based on Organic–Inorganic Lead Bromide Perovskite. *J. Phys. Chem. Lett.* **2013**, *4*, 897–902.
- (15) Dymshits, A.; Rotem, A.; Etgar, L. High Voltage in Hole Conductor Free Organo Metal Halide Perovskite Solar Cells. *J. Mater. Chem. A* **2014**, *2*, 20776–20781.
- (16) Kulbak, M.; Cahen, D.; Hodes, G. How Important Is the Organic Part of Lead Halide Perovskite Photovoltaic Cells? Efficient CsPbBr₃ Cells. *J. Phys. Chem. Lett.* **2015**, *6*, 2452–2456.
- (17) Yantara, N.; Bhaumik, S.; Yan, F.; Sabba, D.; Dewi, H. A.; Mathews, N.; Boix, P. P.; Demir, H. V.; Mhaisalkar, S. Inorganic Halide Perovskites for Efficient Light-Emitting Diodes. *J. Phys. Chem. Lett.* **2015**, *6*, 4360–4364.
- (18) Grancini, G.; Srimath Kandada, A. R.; Frost, J. M.; Barker, A. J.; De Bastiani, M.; Gandini, M.; Marras, S.; Lanzani, G.; Walsh, A.; Petrozza, A. Role of Microstructure in the Electron–Hole Interaction of Hybrid Lead Halide Perovskites. *Nat. Photonics* **2015**, *9*, 695–701.
- (19) Yun, J. S.; Ho-Baillie, A.; Huang, S.; Woo, S. H.; Heo, Y.; Seidel, J.; Huang, F.; Cheng, Y.-B.; Green, M. A. Benefit of Grain Boundaries in Organic–Inorganic Halide Planar Perovskite Solar Cells. *J. Phys. Chem. Lett.* **2015**, *6*, 875–880.
- (20) Huang, J.; Shao, Y.; Dong, Q. Organometal Trihalide Perovskite Single Crystals: A Next Wave of Materials for 25% Efficiency Photovoltaics and Applications Beyond? *J. Phys. Chem. Lett.* **2015**, *6*, 3218–3227.
- (21) Shi, D.; et al. Low Trap-State Density and Long Carrier Diffusion in Organolead Trihalide Perovskite Single Crystals. *Science* **2015**, *347*, 519–522.
- (22) Dong, Q.; Fang, Y.; Shao, Y.; Mulligan, P.; Qiu, J.; Cao, L.; Huang, J. Electron-Hole Diffusion Lengths > 175 μm in Solution-Grown CH₃NH₃PbI₃ Single Crystals. *Science* **2015**, *347*, 967–970.
- (23) Zhao, P.; Xu, J.; Dong, X.; Wang, L.; Ren, W.; Bian, L.; Chang, A. Large-Size CH₃NH₃PbBr₃ Single Crystal: Growth and in Situ Characterization of the Photophysics Properties. *J. Phys. Chem. Lett.* **2015**, *6*, 2622–2628.
- (24) Kunugita, H.; et al. Excitonic Feature in Hybrid Perovskite CH₃NH₃PbBr₃ Single Crystals. *Chem. Lett.* **2015**, *44*, 852–854.
- (25) Fang, H.-H.; Raissa, R.; Abdu-Aguye, M.; Adjokatse, S.; Blake, G. R.; Even, J.; Loi, M. A. Photophysics of Organic–Inorganic Hybrid Lead Iodide Perovskite Single Crystals. *Adv. Funct. Mater.* **2015**, *25*, 2378–2385.
- (26) Yamada, Y.; Yamada, T.; Phuong, L. Q.; Maruyama, N.; Nishimura, H.; Wakamiya, A.; Murata, Y.; Kanemitsu, Y. Dynamic Optical Properties of CH₃NH₃PbI₃ Single Crystals as Revealed by One- and Two-Photon Excited Photoluminescence Measurements. *J. Am. Chem. Soc.* **2015**, *137*, 10456–10459.
- (27) Grancini, G.; D’Innocenzo, V.; Dohner, E. R.; Martino, N.; Srimath Kandada, A. R.; Mosconi, E.; De Angelis, F.; Karunadasa, H. I.; Hoke, E. T.; Petrozza, A. CH₃NH₃PbI₃ Perovskite Single Crystals: Surface Photophysics and Their Interaction with the Environment. *Chemical Science* **2015**, *6*, 7305–7310.
- (28) Yang, Y.; Yan, Y.; Yang, M.; Choi, S.; Zhu, K.; Luther, J. M.; Beard, M. C. Low Surface Recombination Velocity in Solution-Grown CH₃NH₃PbBr₃ Perovskite Single Crystal. *Nat. Commun.* **2015**, *6*, 7961–7966.
- (29) Zhang, T.; Yang, M.; Benson, E. E.; Li, Z.; van de Lagemaat, J.; Luther, J. M.; Yan, Y.; Zhu, K.; Zhao, Y. A Facile Solvothermal Growth of Single Crystal Mixed Halide Perovskite CH₃NH₃Pb(Br_(1-x)Cl_x)₃. *Chem. Commun.* **2015**, *51*, 7820–7823.
- (30) Brittman, S.; Garnett, E. C. Measuring n and k at the Microscale in Single Crystals of CH₃NH₃PbBr₃ Perovskite. *J. Phys. Chem. C* **2016**, *120*, 616–620.
- (31) Dingley, D. J.; Randle, V. Microtexture Determination by Electron Back-Scatter Diffraction. *J. Mater. Sci.* **1992**, *27*, 4545–4566.
- (32) Schwartz, A. J.; Kumar, M.; Adams, B. L.; Field, D. P. *Electron Backscatter Diffraction in Materials Science*; Springer: New York, 2009; Vol. 2.
- (33) Schulz, P.; Edri, E.; Kirmayer, S.; Hodes, G.; Cahen, D.; Kahn, A. Interface Energetics in Organo-Metal Halide Perovskite-Based Photovoltaic Cells. *Energy Environ. Sci.* **2014**, *7*, 1377–1381.
- (34) Goldmann, A.; Landolt, H.; Börnstein, R. *Electronic Structure of Solids: Photoemission Spectra and Related Data*; Springer: New York, 1994.
- (35) Chueh, C.-C.; Li, C.-Z.; Jen, A. K. Y. Recent Progress and Perspective in Solution-Processed Interfacial Materials for Efficient and Stable Polymer and Organometal Perovskite Solar Cells. *Energy Environ. Sci.* **2015**, *8*, 1160–1189.
- (36) Shi, T.; Yin, W.-J.; Hong, F.; Zhu, K.; Yan, Y. Unipolar Self-Doping Behavior in Perovskite CH₃NH₃PbBr₃. *Appl. Phys. Lett.* **2015**, *106*, 103902.
- (37) Kedem, N.; Brenner, T. M.; Kulbak, M.; Schaefer, N.; Levchenko, S.; Levine, I.; Abou-Ras, D.; Hodes, G.; Cahen, D. Light-Induced Increase of Electron Diffusion Length in a P–N Junction Type CH₃NH₃PbBr₃ Perovskite Solar Cell. *J. Phys. Chem. Lett.* **2015**, *6*, 2469–2476.